

Electronic Supplementary Information for

On the Shape Transformation of a Pine Cone Scales

Received 00th January 20xx,
Accepted 00th January 20xx

DOI: 10.1039/x0xx00000x

Sen Lin^a, Yi Min Xie^a, Qing Li^b, Xiaodong Huang^a, and Shiwei Zhou^{a†}

www.rsc.org/

1. Rayleigh-Ritz Method

To relate the principal curvatures to the temperature, we deploy the theory based on the Rayleigh-Ritz method²⁴. The displacement u_1 , u_2 and u_3 of the neutral plane in x , y and z directions, respectively, can be assumed as

$$\begin{aligned} u_1 &= A_1x + A_2x^3 + A_3xy^2 \\ u_2 &= B_1y + B_2y^3 + B_3yx^2 \\ u_3 &= -\kappa_x x^2/2 - \kappa_y y^2/2 \end{aligned} \quad (S1)$$

where x , y and z are the coordinates in a Cartesian system. κ_x and κ_y are the longitudinal and transversal principal curvatures. A_i and B_i are the parameters determined by the minimum potential energy of the deformation. The total strain $\varepsilon_{\alpha\beta}$ ($\alpha, \beta = 1$ or 2) can be calculated by the Von-Karman formulas

$$\begin{aligned} \varepsilon_{\alpha\beta} &= \frac{1}{2} \left(\frac{\partial u_\alpha}{\partial x_\beta} + \frac{\partial u_\beta}{\partial x_\alpha} + \frac{\partial u_3}{\partial x_\alpha} \frac{\partial u_3}{\partial x_\beta} \right) + z\kappa_{\alpha\beta} \\ \Rightarrow \begin{cases} \varepsilon_{11} = A_1 + 3A_2x^2 + A_3y^2 + \kappa_x^2 x^2/2 + z\kappa_x \\ \varepsilon_{22} = B_1 + 3B_2y^2 + B_3x^2 + \kappa_y^2 y^2/2 + z\kappa_y \\ \varepsilon_{12} = (A_3 + B_3)xy + \kappa_x \kappa_y xy/2 \end{cases} \end{aligned} \quad (S2)$$

For an isotropic and homogeneous Kirchhoff plate²², the stress-strain relation can be expressed as that the stress $\sigma_{13} = \sigma_{23} = \sigma_{33} = 0$, and the rest components are represented as

$$\begin{bmatrix} \sigma_{11} \\ \sigma_{22} \\ \sigma_{12} \end{bmatrix} = \frac{E_i}{(1-\mu^2)} \begin{bmatrix} 1 & \mu & 0 \\ \mu & 1 & 0 \\ 0 & 0 & (1-\mu)/2 \end{bmatrix} \begin{bmatrix} \varepsilon_{11} \\ \varepsilon_{22} \\ 2\varepsilon_{12} \end{bmatrix} - \frac{E_i \alpha_i P}{(1-\mu)} \begin{bmatrix} 1 \\ 1 \\ 0 \end{bmatrix} \quad (S3)$$

The strain resulted from the mechanical loading (known as elastic strain) are given as:

$$\begin{bmatrix} \varepsilon_{11}^m \\ \varepsilon_{22}^m \\ 2\varepsilon_{12}^m \end{bmatrix} = \frac{1}{E_i} \begin{bmatrix} 1 & -\mu & 0 \\ -\mu & 1 & 0 \\ 0 & 0 & 2(1+\mu) \end{bmatrix} \begin{bmatrix} \sigma_{11} \\ \sigma_{22} \\ \sigma_{12} \end{bmatrix} \quad (S4)$$

The strain energy U and the bending energy U_b density are obtained as

$$U = \sum \frac{1}{2} \sigma_{ij} \varepsilon_{ij}^m \quad (S5)$$

$$U_b = \frac{E_i h_i^2}{8(1-\mu^2)} \left[(\kappa_x + \kappa_y)^2 - 2(1-\mu)\kappa_x \kappa_y \right] \quad (S6)$$

In this case, the total strain energy U_t and the bending energy U_{bt} can be obtained by integrating across the thickness direction z (the Young's moduli and the humidity expansion coefficients for these two layers are denoted as $E_1, E_2, \alpha_1, \alpha_2$, respectively)

$$\begin{cases} U_t = \int_0^h \int_{-L_2}^{L_2} \int_{-L_1}^{L_1} U_{s1}(E_1, \alpha_1) dx dy dz + \int_0^h \int_{-L_2}^{L_2} \int_{-L_1}^{L_1} U_{s2}(E_2, \alpha_2) dx dy dz \\ U_{bt} = \int_0^h \int_{-L_2}^{L_2} \int_{-L_1}^{L_1} U_{b1}(E_1, \alpha_1) dx dy dz + \int_0^h \int_{-L_2}^{L_2} \int_{-L_1}^{L_1} U_{b2}(E_2, \alpha_2) dx dy dz \end{cases} \quad (S7)$$

As a consequence, the total stretching energy U_{st} is calculated from

$$U_{st} = U_t - U_{bt} \quad (S8)$$

By solving the equations $\partial U / \partial A_i = 0$, $\partial U / \partial B_i = 0$, $\partial U / \partial \kappa_x = 0$, $\partial U / \partial \kappa_y = 0$, the same group of equations as Eqs. (9-14) can be obtained. In this case, substituting $h = 1.1$ mm, $2L_1 = 31.2$ mm, κ_x and κ_y (Eqs. 13-14) back into Eqs. (S7-S8), we obtain the bending and the stretching energies map as Fig. S1.

^a Centre for Innovative Structures and Materials, School of Engineering, RMIT University, GPO Box 2476, Melbourne 3001, Australia. Email: shiwei.zhou@rmit.edu.au. Telephone +61 3 9925 2098. Facsimile +61 3 9639 0138

^b School of Aerospace, Mechanical and Mechatronics Engineering, The University of Sydney, NSW 2006, Australia.

† Footnotes relating to the title and/or authors should appear here.

Electronic Supplementary Information (ESI) available: [details of any supplementary information available should be included here]. See DOI: 10.1039/x0xx00000x

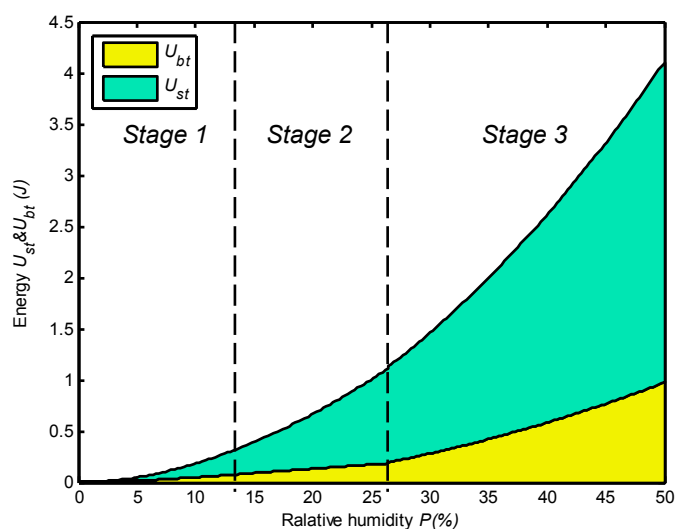


Fig. S1. The bending energy and the stretching energy versus the relative humidity.

According to Fig. S1, the stretching energy increases nonlinearly at stages 1 and 2, while the bending energy keeps rising almost linearly. These two strain energy components both increase at a higher rate after the critical humidity. Additionally, the stretching dominates the deformation by occupying about 75% of the total strain energy.

2 Curvature Variation under Constant Humidity

To investigate the behavior of pine cones in some conditions like heavy rainstorm or raindrops spatter on scales, a physical experiment was designed. By exposed in the enclosed cabinet in 23°C and 45% humidity for 5 hours, the same sample mentioned in the discussion ($h = 1.1$ mm, $2L_1 = 31.2$ mm) was pre-treated into a flattened plate. The sample was taken out for 3D scanning and then returned into the cabinet, where the humidity had been increase to 95% directly and the temperature kept constant. Afterwards, the sample was drawn from cabinet to record the deformation per hour. The test lasted 10 hours in total, and then the curvature variation with respect to time (t) could be represented as Fig. S2.

To illustrate, the trend of curvature variation is quite similar to Fig. 4, where the humidity P is replaced by time t . To compare with the theoretical results and explain this time-domain curvature variation, we introduce the moisture content factor $\theta = P/t = 0.06$ h⁻¹, which converts the moisture content of the scale in 95% humidity into that in the corresponding humidity 45%, 50%, 55%, etc. The test and theoretical results obtained by substituting the relative humidity P with θt in Eqs. (13-14) are plotted in Fig. S2, which shows they are marginally equal.

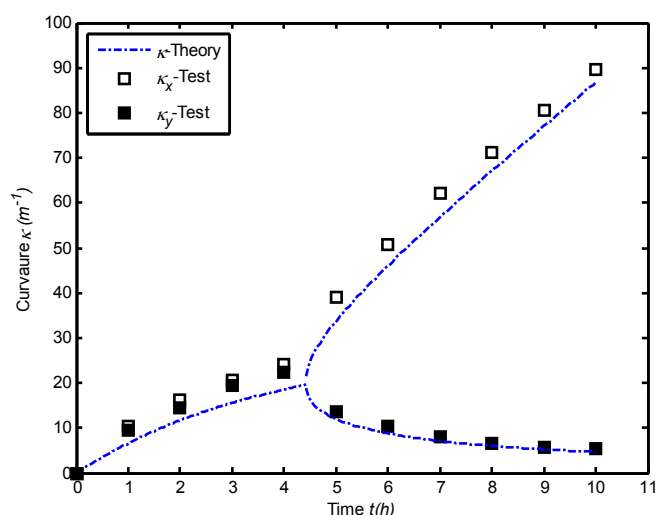


Fig. S2. The longitudinal and transversal principle curvatures fluctuate versus the relative humidity. The theoretical result, the experimental results of κ_x and κ_y are represented by blue line, empty and solid dots, respectively.

Fig. S2 shows a quite similar trend to that of Fig. 4 in the main context, which is in good agreement with the theoretical results. However, the principal curvatures κ_x and κ_y measured in the test are slightly greater than the theoretical values. The main reason could be attributed to the length of physical sample is smaller than the numerical model. As discussed in the main context, short scale generally leads to large κ_x and κ_y in the bending progress. On the other side, the critical time t^* (corresponding to the critical humidity P^*) in the experiment is slightly smaller than the theoretical value, which conflicts with $t^* \sim (h/L_1)^2$. The reason could be that the water content in the scales increases nonlinearly with respect to time. It rises rapidly at the beginning of test and reaches the critical value earlier than theoretical prediction. Once the moisture difference between the scales and the environment is reduced, the water absorbability would be weakened, which results in the final appearance of the scale being similar to the one shown in Fig. 5h.